Cent. Eur. J. Phys. • 7(3) • 2009 • 555-567
DOI: 10.2478/s11534-009-0016-x

VERSITA

Central European Journal of **Physics**

Magnetic properties of the mixed spin-5/2 and spin-3/2 Blume-Capel Ising system on the two-fold Cayley tree

Research Article

Rachidi A. Yessoufou, Saliou H. Amoussa, Felix Hontinfinde*

Département de Physique (FAST) et Institut de Mathématiques et de Sciences Physiques (IMSP)
Université d'Abomey-Calavi, 01 BP 613, Porto-Novo, Bénin

Received 20 November 2008; accepted 23 January 2009

Abstract: We use exact recursion relations to study the magnetic properties of the half-integer mixed spin-5/2 and spin-3/2 Blume-Capel Ising ferromagnetic system on the two-fold Cayley tree that consists of two sublattices A and B. Two positive crystal-field interactions Δ_1 and Δ_2 are considered for the sublattice with spin-5/2 and spin-3/2 respectively. For different coordination numbers q of the Cayley tree sites, the phase diagrams of the model are presented with a special emphasis on the case $q = 3$, since other values of q reproduce similar results. First, the $T = 0$ phase diagram is illustrated in the $(D_A = \Delta_1/J, D_B = \Delta_2/J)$ plane of reduced crystal-field interactions. This diagram shows triple points and coexistence lines between thermodynamically stable phases. Secondly, the thermal variation of the magnetization belonging to each sublattice for some coordination numbers q are investigated as well as the Helmoltz free energy of the system. First-order and second-order phase transitions are found. The second-order phase transitions become sharper and sharper when D_A or D_B increases. The first-order transitions only exist for some appropriate non-zero values of D_A and/or D_B. The corresponding transition lines never connect to the second-order transition lines. Thus, the non-existence of tricritical points remains one of the key features of the present model. The magnetic exponent β_0 of the model is estimated and found to be $\frac{1}{4}$ at small values of $D_A = D_B = D$ and $\beta_0 = \frac{1}{2}$ at large values of D. At intermediate values of D, there is a crossover region where the magnetic exponent displays interesting behaviours.

PACS (2008): 05.50.+q; 05.70.Ce; 64.60.Cn; 75.10.Hk; 75.30.Gw

Keywords: mixed spin model • two-fold cayley tree • recursion relations • magnetization • phase transition

1. Introduction

Mixed Ising spin systems have attracted much interest over the few past years from both theoretical and experimental point of view. This is due to their relevance in studying molecular-based magnetic materials which exhibit ferrimagnetic properties [1] and also to their technological applications in the domain of thermomagnetic recording [2]. Mixed Ising spin models appear simpler in describing systems that exhibit a tricritical point (TCP) behaviour [3, 4]. Moreover, they are useful to study the effect of inhomogeneities on the phase diagram of Ising systems. When defined on hierarchical graphs as the Bethe lattice or the Cayley tree, interesting statistical properties

*E-mail: fhontinfinde@yahoo.fr

are expected. In these cases, some exact treatments [4–6] are possible even at high spin values. Half-integer spin models are more exciting because first, they are less studied and second, they can show multicritical behaviour or a magnetoelastic transition or instability [7].

The properties of such Ising systems have been studied by well-known methods of equilibrium statistical mechanics such as the mean-field approximation (MFA) [3], the effective-field theory (EFT) [8, 9], Monte Carlo simulations [10], cluster variation method (CVM) [11], the renormalization group approach [12], exact calculations,..*etc* (see [5, 6, 13] and references therein). Ekiz studied the mixed spin-$\frac{1}{2}$ and spin-1 on the two-fold Cayley tree [14–16] by means of exact recursion relations and found a tricritical point for some values of the coordination number q [4]. More recently, Zhang and Kong [13] used the same technique to investigate the mixed spin-$\frac{3}{2}$ and spin-$\frac{1}{2}$ Blume-Capel model on the same Cayley lattice. The presence of lattice anisotropy (or crystal-field interaction) in this model is interesting since it might induce a profound influence on the molecular magnetism of this system. They obtained interesting results such as the exact phase diagram of the model and the non-existence of a TCP. The next possible mixed half-integer spin model includes the mixed spin-$\frac{3}{2}$ and spin-$\frac{5}{2}$. This model has been studied by Zhang *et al.* [17] in its ferrimagnetic version with an interlayer coupling and a simple approach to calculate the internal energy of the system was proposed. Recently, Albayrak and Yigit analyzed the mixed spin-$\frac{3}{2}$ and spin-$\frac{5}{2}$ Blume-Capel model on the Bethe lattice [18]. Although the model is exclusively theoretical, they obtained interesting results for the ferrimagnetic case ($J < 0$), with the existence of first and second order transitions as well as compensation transitions for appropriate values of the crystal-field.

In this paper, we present an exact formulation of the previous model in its ferromagnetic version on the two-fold Cayley tree using exact recursion relations. The two-fold Cayley tree consists of two sublattices A and B. Two positive crystal-fields are considered with Δ_1 on sublattice A and Δ_2 on sublattice B. Here, the spin-$\frac{5}{2}$ and spin-$\frac{3}{2}$ are respectively put on sublattices A and B and this considerably increases the number and the complexity of analytical recursion relations needed to compute thermodynamic quantities of interest. We would like to know how this increasing number of possible spin states and the difference in the sublattice anisotropies could modify the results found by Zhang and Kong [13] at low spin values. Our calculations give results that can be summarized as follows. When the temperature increases and one of the sublattice anisotropies takes the value zero, or when both crystal-fields have relatively small or large values, the different sublattice magnetizations tend continuously to zero with no anomalous behaviour in the free energy of the system. Thus, in these cases, the ferro-para phase transition is exclusively of second order as found in reference [13]. At intermediate values of the crystal-field strengths, the Helmoltz free energy and the sublattice magnetizations show a discontinuity at low temperarure before the second order transition (SOT) temperature. This temperature at which the free energy appears non-analytic is attributed to a first-order transition (FOT). Different numerical investigations indicate the non-existence of a tricritical point in the model since the FOT lines never connect to the SOT lines. The phase diagrams are presented in the model parameters' space. In particular, the case where the two sublattices have the same crystal-field strengths. At high temperature and large sublattice anisotropy, the system is completely in the paramagnetic phase. At low temperature and small (or large) values of the crystal-field, the system is in one of the thermodynamically stable phases depicted in the $T = 0$ phase diagram. The second order transition region is analyzed by estimating the magnetic exponent β_0. We find that in the particular case where both sublattice anisotropies have equal strength D, β_0 displays two limiting values $\frac{1}{4}$ and $\frac{1}{2}$ when D increases. The different calculations are made with double precision and the accuracy set at least to 10^{-6} for the convergence of different quantities.

The remainder of this paper is organized as follows. In section 2, the formulation of the problem is given. In section 3, the exact expressions of the sublattice magnetizations are obtained. There, the phase diagrams of the model and the behaviour of the magnetic exponent with D are illustrated. Section 4 is devoted to the conclusions. In the Appendix, the explicit expression of the free energy is given as well as the expressions of some recursion relations.

2. The formulation of the problem

2.1. Definition of the model

The two-fold Cayley tree is constructed as follows. First, we consider two points O and O' as the central points of the graph (see Fig. 1) [13]. The "first shell" of the graph is obtained by constructing q points that connect to each central point. For the central point O, one gets the "first left shell" whereas for O', one obtains the first opposite shell named "the first right shell". The graph grows further from these q points by connection to $(q-1)$ new points and so on. At the end, one has a two-fold Cayley tree with a frontier shell (absent in the Bethe lattice) that has closed loops. The two-fold Cayley tree consists of two

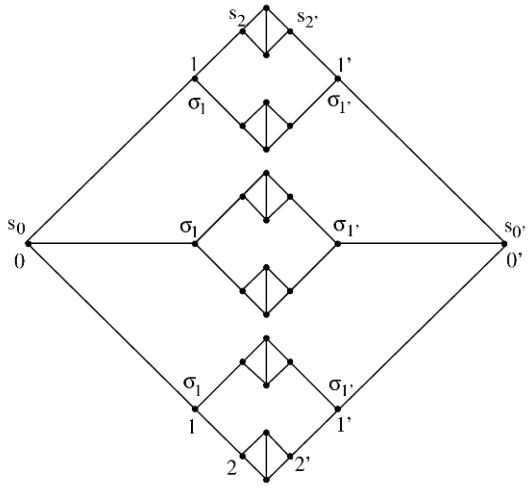

Figure 1. A two-fold Cayley tree with coordination number $q = 3$ and generation $n = 3$. Spins σ are defined on sublattice B. The central spins are denoted by spins s_0 and $s_{0'}$.

sublattices A and B.

Discrete Spin variables are put on the Cayley-tree with spin-$\frac{5}{2}$ on sublattice A (variable s) and spin-$\frac{3}{2}$ on sublattice B (variable σ). Then, $s_i = \pm\frac{5}{2}, \pm\frac{3}{2}, \pm\frac{1}{2}$ and $\sigma_j = \pm\frac{3}{2}, \pm\frac{1}{2}$ are the possible spin variables on sites of the two sublattices.

The interaction Hamiltonian of this mixed spin system is defined as:

$$H = -J\sum_{\langle ij\rangle} s_i\sigma_j + \Delta_1\sum_i s_i^2 + \Delta_2\sum_j \sigma_j^2, \qquad (1)$$

where $J > 0$ is the ferromagnetic nearest-neighbour exchange coupling constant, Δ_1 and Δ_2 are the crystal-field or lattice anisotropy for spin-$\frac{5}{2}$ and spin-$\frac{3}{2}$ respectively. In this equation, the first sum runs over nearest-neighbour spin pairs; the second over sites of the sublattice A and the third over sites of the sublattice B.

The partition function of this mixed spin system is given by:

$$Z = \sum e^{-\beta H} = \sum_{(s,\sigma)} e^{\beta\left(J\sum_{\langle ij\rangle} s_i\sigma_j - \Delta_1\sum_i s_i^2 - \Delta_2\sum_j \sigma_j^2\right)} \qquad (2)$$

where $\beta = 1/kT$, with k the Boltzmann constant and T the temperature. The magnetizations are computed from some exact recursion relations that we treated by means of an iteration procedure. In fact, the graph splits into q disconnected pieces when cut at the central points O and O'. Therefore the partition function can be written as follows:

$$Z = \sum_{s_O}\sum_{s_{O'}} e^{-\beta\Delta_1\left(s_O^2 + s_{O'}^2\right)}\left[g_n(s_O, s_{O'})\right]^q, \qquad (3)$$

where s_0 and $s_{0'}$ are the central spin values and $g_n(s_O, s_{O'})$ denotes the partition function of an individual branch. Its explicit expression reads:

$$g_n(s_O, s_{O'}) = \sum_{\sigma_1}\sum_{\sigma_{1'}} \exp\left[\beta\left(Js_O\sigma_1 + Js_{O'}\sigma_{1'} - \Delta_2(\sigma_1^2 + \sigma_{1'}^2) + J\sum_{\langle ij\rangle} s_i\sigma_j - \Delta_1\sum_i s_i^2 - \Delta_2\sum_j \sigma_j^2\right)\right]. \qquad (4)$$

Each branch can be cut on the sites σ_1 or $\sigma_{1'}$, which are the nearest and the next-nearest to the central points, respectively. Thus, one gets the following recurrence relations for $g_n(s_O, s_{O'})$ and $g_{n-1}(\sigma_1, \sigma_{1'})$:

$$g_n(s_0, s_{0'}) = \sum_{\sigma_1}\sum_{\sigma_{1'}} e^{\left[\beta\left(Js_0\sigma_1 + Js_{0'}\sigma_{1'} - \Delta_2\left(\sigma_1^2 + \sigma_{1'}^2\right)\right)\right]}\left[g_{n-1}(\sigma_1, \sigma_{1'})\right]^{q-1}, \qquad (5)$$

and

$$g_{n-1}(\sigma_1, \sigma_{1'}) = \sum_{s_2}\sum_{s_{2'}} e^{\left[\beta\left\{J\sigma_1 s_2 + J\sigma_{1'}s_{2'} - \Delta_1\left(s_2^2 + s_{2'}^2\right)\right\}\right]}\left[g_{n-2}(s_2, s_{2'})\right]^{q-1}. \qquad (6)$$

Thus, for $g_n\left(\frac{5}{2}, \frac{5}{2}\right)$ and $g_{n-1}\left(\frac{3}{2}, \frac{3}{2}\right)$ as examples, the explicit expressions read:

$$g_n\left(\frac{5}{2}, \frac{5}{2}\right) = e^{\beta\left(\frac{15}{2}J - \frac{9}{2}\Delta_2\right)} g_{n-1}^{q-1}\left(\frac{3}{2}, \frac{3}{2}\right) + 2e^{-\frac{9}{2}\beta\Delta_2} g_{n-1}^{q-1}\left(\frac{3}{2}, -\frac{3}{2}\right) + 2e^{\beta\left(5J - \frac{5}{2}\Delta_2\right)} g_{n-1}^{q-1}\left(\frac{3}{2}, \frac{1}{2}\right) + 2e^{\beta\left(\frac{5J}{2} - \frac{5}{2}\Delta_2\right)} g_{n-1}^{q-1}\left(\frac{3}{2}, -\frac{1}{2}\right) + e^{\beta\left(-\frac{15}{2}J - \frac{9}{2}\Delta_2\right)} g_{n-1}^{q-1}\left(-\frac{3}{2}, -\frac{3}{2}\right)$$

$$
\begin{aligned}
&+2e^{\beta\left(-\frac{5J}{2}-\frac{5}{2}\Delta_2\right)}g_{n-1}^{q-1}\left(-\frac{3}{2},\frac{1}{2}\right)+2e^{\beta\left(-5J-\frac{5}{2}\Delta_2\right)}g_{n-1}^{q-1}\left(-\frac{3}{2},-\frac{1}{2}\right)+e^{\beta\left(\frac{5}{2}J-\frac{1}{2}\Delta_2\right)}g_{n-1}^{q-1}\left(\frac{1}{2},\frac{1}{2}\right)\\
&+2e^{-\frac{1}{2}\beta\Delta_2}g_{n-1}^{q-1}\left(\frac{1}{2},-\frac{1}{2}\right)+e^{\beta\left(-\frac{5}{2}J-\frac{1}{2}\Delta_2\right)}g_{n-1}^{q-1}\left(-\frac{1}{2},-\frac{1}{2}\right),\\
g_{n-1}\left(\frac{3}{2},\frac{3}{2}\right) &= e^{\frac{15\beta J}{2}}e^{-\frac{25\beta\Delta_1}{2}}g_{n-2}^{q-1}\left(\frac{5}{2},\frac{5}{2}\right)+2e^{-\frac{25\beta\Delta_1}{2}}g_{n-2}^{q-1}\left(\frac{5}{2},-\frac{5}{2}\right)+2e^{6\beta J}e^{-\frac{17\beta\Delta_1}{2}}g_{n-2}^{q-1}\left(\frac{5}{2},\frac{3}{2}\right)\\
&+2e^{\frac{3\beta J}{2}}e^{-\frac{17\beta\Delta_1}{2}}g_{n-2}^{q-1}\left(\frac{5}{2},-\frac{3}{2}\right)+2e^{\frac{9\beta_1 J}{2}}e^{-\frac{13\beta\Delta_1}{2}}g_{n-2}^{q-1}\left(\frac{5}{2},\frac{1}{2}\right)+2e^{3\beta J}e^{-\frac{13\beta\Delta_1}{2}}g_{n-2}^{q-1}\left(\frac{5}{2},-\frac{1}{2}\right)\\
&+e^{-\frac{15\beta J}{2}}e^{-\frac{25\beta\Delta_1}{2}}g_{n-2}^{q-1}\left(-\frac{5}{2},-\frac{5}{2}\right)+2e^{-\frac{3\beta J}{2}}e^{-\frac{17\beta\Delta_1}{2}}g_{n-2}^{q-1}\left(-\frac{5}{2},\frac{3}{2}\right)+2e^{-6\beta J}e^{-\frac{17\beta\Delta_1}{2}}g_{n-2}^{q-1}\left(-\frac{5}{2},-\frac{3}{2}\right)\\
&+2e^{-3\beta J}e^{-\frac{13\beta\Delta_1}{2}}g_{n-2}^{q-1}\left(-\frac{5}{2},\frac{1}{2}\right)+2e^{-\frac{9\beta J}{2}}e^{-\frac{13\beta\Delta_1}{2}}g_{n-2}^{q-1}\left(-\frac{5}{2},-\frac{1}{2}\right)+e^{\frac{9\beta J}{2}}e^{-\frac{9\beta\Delta_1}{2}}g_{n-2}^{q-1}\left(\frac{3}{2},\frac{3}{2}\right)\\
&+2e^{-\frac{9\beta\Delta_1}{2}}g_{n-2}^{q-1}\left(\frac{3}{2},-\frac{3}{2}\right)+2e^{3\beta J}e^{-\frac{5\beta\Delta_1}{2}}g_{n-2}^{q-1}\left(\frac{3}{2},\frac{1}{2}\right)\\
&+2e^{\frac{3\beta J}{2}}e^{-\frac{5\beta\Delta_1}{2}}g_{n-2}^{q-1}\left(\frac{3}{2},-\frac{1}{2}\right)+e^{-\frac{9\beta J}{2}}e^{-\frac{9\beta\Delta_1}{2}}g_{n-2}^{q-1}\left(-\frac{3}{2},-\frac{3}{2}\right)\\
&+2e^{-\frac{3\beta J}{2}}e^{-\frac{5\beta\Delta_1}{2}}g_{n-2}^{q-1}\left(-\frac{3}{2},\frac{1}{2}\right)+2e^{-3\beta J}e^{-\frac{5\beta\Delta_1}{2}}g_{n-2}^{q-1}\left(-\frac{3}{2},-\frac{1}{2}\right)+e^{\frac{3\beta J}{2}}e^{-\frac{\beta\Delta_1}{2}}g_{n-2}^{q-1}\left(\frac{1}{2},\frac{1}{2}\right)\\
&+2e^{-\frac{\beta\Delta_1}{2}}g_{n-2}^{q-1}\left(\frac{1}{2},-\frac{1}{2}\right)+e^{-\frac{3\beta J}{2}}e^{-\frac{\beta\Delta_1}{2}}g_{n-1}^{q-1}\left(-\frac{1}{2},-\frac{1}{2}\right).
\end{aligned}
$$

2.2. Definition of new variables

The number of recursion relations is considerably reduced due to the symmetry of the Cayley tree around the frontier shell. This symmetry induces symmetric relations for g_n and g_{n-1} as follows:

$$g_n(s_0,s_{0'})=g_n(s_{0'},s_0), \tag{7}$$

$$g_{n-1}(\sigma_1,\sigma_{1'})=g_{n-1}(\sigma_{1'},\sigma_1). \tag{8}$$

New variables $h_{n-1}(\sigma_1,\sigma_{1'})$ and $h_n(s_0,s_{0'})$ are introduced by renormalizing g_{n-1} and g_n by $g_{n-1}(3/2,3/2)$ and $g_n(-1/2,-1/2)$ respectively. In the following, we consider:

$$
\begin{aligned}
A_{n-1}&=h_{n-1}\left(\frac{3}{2},-\frac{3}{2}\right); & B_{n-1}&=h_{n-1}\left(\frac{3}{2},\frac{1}{2}\right);\\
C_{n-1}&=h_{n-1}\left(\frac{3}{2},-\frac{1}{2}\right); & D_{n-1}&=h_{n-1}\left(-\frac{3}{2},-\frac{3}{2}\right);\\
E_{n-1}&=h_{n-1}\left(-\frac{3}{2},\frac{1}{2}\right); & F_{n-1}&=h_{n-1}\left(-\frac{3}{2},-\frac{1}{2}\right);\\
G_{n-1}&=h_{n-1}\left(\frac{1}{2},\frac{1}{2}\right); & H_{n-1}&=h_{n-1}\left(\frac{1}{2},-\frac{1}{2}\right);
\end{aligned}
$$

$$
\begin{aligned}
I_{n-1}&=h_{n-1}\left(-\frac{1}{2},-\frac{1}{2}\right); & J_n&=h_n\left(\frac{5}{2},\frac{5}{2}\right);\\
K_n&=h_n\left(\frac{5}{2},-\frac{5}{2}\right); & L_n&=h_n\left(\frac{5}{2},\frac{3}{2}\right);\\
M_n&=h_n\left(\frac{5}{2},-\frac{3}{2}\right); & N_n&=h_n\left(\frac{5}{2},\frac{1}{2}\right);\\
O_n&=h_n\left(\frac{5}{2},-\frac{1}{2}\right); & P_n&=h_n\left(-\frac{5}{2},-\frac{5}{2}\right);\\
Q_n&=h_n\left(-\frac{5}{2},\frac{3}{2}\right); & R_n&=h_n\left(-\frac{5}{2},-\frac{3}{2}\right);\\
S_n&=h_n\left(-\frac{5}{2},\frac{1}{2}\right); & T_n&=h_n\left(-\frac{5}{2},-\frac{1}{2}\right);\\
U_n&=h_n\left(\frac{3}{2},\frac{3}{2}\right); & V_n&=h_n\left(\frac{3}{2},-\frac{3}{2}\right);\\
W_n&=h_n\left(\frac{3}{2},\frac{1}{2}\right); & X_n&=h_n\left(\frac{3}{2},-\frac{1}{2}\right);\\
Y_n&=h_n\left(-\frac{3}{2},-\frac{3}{2}\right); & Z_n&=h_n\left(-\frac{3}{2},\frac{1}{2}\right);\\
\gamma_n&=h_n\left(-\frac{3}{2},-\frac{1}{2}\right); & \beta_n&=h_n\left(\frac{1}{2},\frac{1}{2}\right);\\
\alpha_n&=h_n\left(\frac{1}{2},-\frac{1}{2}\right).
\end{aligned}
$$

2.3. Expressions of the sublattice magnetizations

By definition, the average value of a physical variable $(\cdot)$ inside a spin box Λ with specified boundary conditions

(b.c) is formally written as:

$$\langle(\cdot)\rangle_{\Lambda}^{b.c} = Z_{\Lambda}^{b.c\,-1} \sum_{\sigma\in\Omega_{\Lambda}} (\cdot) e^{-\beta H_{\Lambda}(\sigma/b.c)} \tag{9}$$

where $Z_{\Lambda}^{b.c}$ is the partition function, σ an element of the space configuration Ω_{Λ}. Thus, the expressions of the sublattice magnetizations M_A and M_B are:

$$M_A = Z_A^{-1} \sum_{s_O} \sum_{s_{O'}} s_O e^{-\beta\Delta_1\left(s_O^2+s_{O'}^2\right)} [g_n\,(s_O, s_{O'})]^q, \tag{10}$$

$$M_B = Z_B^{-1} \sum_{\sigma_1} \sum_{\sigma_{1'}} \sigma_1 e^{-\beta\Delta_2\left(\sigma_1^2+\sigma_{1'}^2\right)} [g_{n-1}\,(\sigma_1, \sigma_{1'})]^q\,, \tag{11}$$

where

$$Z_A = \sum_{s_O} \sum_{s'_O} e^{-\beta\Delta_1\left\{s_O^2+s_{O'}^1\right\}} [g_n\,(s_O, s_{O'})]^q \tag{12}$$

and

$$Z_B = \sum_{\sigma_1} \sum_{\sigma_{1'}} e^{-\beta\Delta_2\left(\sigma_1^2+\sigma_{1'}^2\right)} [g_{n-1}\,(\sigma_1, \sigma_{1'})]^q\,. \tag{13}$$

By setting $M_A = \dfrac{M'_A}{M^0_A}$ and $M_B = \dfrac{M'_B}{M^0_B}$ one gets the explicit expressions:

$$\begin{aligned} M^0_A &= 2e^{-12\beta\Delta_1} J_n^q + 4e^{-12\beta\Delta_1} K_n^q + 4e^{-8\beta\Delta_1} L_{n-2}^{q-1} + 4e^{-8\beta\Delta_1} M_n^q + 4e^{-6\beta\Delta_1} N_n^q + 4e^{-6\beta\Delta_1} O_n^q \\ &+2e^{-12\beta\Delta_1} P_n^q + 4e^{-8\beta\Delta_1} Q_n^q + 4e^{8\beta\Delta_1} R_n^q + 4e^{-6\beta\Delta_1} S_n^q + 4e^{-6\beta\Delta_1} T_n^q + 2e^{-4\beta\Delta_1} U_n^q + 4e^{-4\beta\Delta_1} V_n^q \\ &+4e^{-2\beta\Delta_1} W_n^q + 4e^{-2\beta\Delta_1} X_n^q + 2e^{-4\beta\Delta_1} Y_n^q + 4e^{-2\beta\Delta_1} Z_n^q + 4e^{-2\beta\Delta_1} \gamma_n^q + 2\beta_n^q + 4\alpha_n^q + 2, \end{aligned}$$

$$\begin{aligned} M'_A &= 5e^{-12\beta\Delta_1} J_n^q + 8e^{-8\beta\Delta_1} L_{n-2}^{q-1} + 2e^{-8\beta\Delta_1} M_n^q + 6e^{-6\beta\Delta_1} N_n^q + 4e^{-6\beta\Delta_1} O_n^q - 5e^{-12\beta\Delta_1} P_n^q - 2e^{-8\beta\Delta_1} Q_n^q \\ &-8e^{-8\beta\Delta_1} R_n^q - 4e^{-6\beta\Delta_1} S_n^q - 6e^{-6\beta\Delta_1} T_n^q + 3e^{-4\beta\Delta_1} U_n^q + 4e^{-2\beta\Delta_1} W_n^q + 2e^{-2\beta\Delta_1} X_n^q - 3e^{-4\beta\Delta_1} Y_n^q \\ &-2e^{-2\beta\Delta_1} Z_n^q - 4e^{-2\beta\Delta_1} \gamma_n^q + \beta_n^q - 1, \end{aligned}$$

$$\begin{aligned} M^0_B &= 2e^{-\frac{9}{2}\beta\Delta_2} \left(1 + D_{n-1}^q + 2A_{n-1}^q\right) + 4e^{-\frac{5}{2}\beta\Delta_2} \left(B_{n-1}^q + C_{n-1}^q + E_{n-1}^q + F_{n-1}^q\right) \\ &+2e^{-\frac{1}{2}\beta\Delta_2} \left(G_{n-1}^q + 2H_{n-1}^q + I_{n-1}^q\right), \end{aligned}$$

$$M'_B = 3e^{-\frac{9}{2}\beta\Delta_2} \left(1 - D_{n-1}^q\right) + 2e^{-\frac{5}{2}\beta\Delta_2} \left(2B_{n-1}^q - 2F_{n-1}^q - E_{n-1}^q + C_{n-1}^q\right) + e^{-\frac{1}{2}\beta\Delta_2} \left(G_{n-1}^q - I_{n-1}^q\right).$$

For fixed values of the model parameters, one starts from some initial values of the recursion relations which are used to compute new values of the relations. The procedure is repeated up to convergence (within some given accuracy) where the magnetizations are calculated.

2.4. Formulation of the critical temperatures

With increasing temperature at fixed other model parameters, the temperature at which the sublattice magnetizations go continuously and simultaneously to zero without any anomalous behaviour in the Helmoltz free energy F (see expression in the Appendix) is taken as the SOT temperature. This so-called Curie Temperature T_c separates the ferromagnetic ordered phase from the disordered paramagnetic phase. Some features of the system at T_c may be obtained by setting M_B^0 to zero, ie by solving the system of equations: $D_{n-1} = 1$, $2B_{n-1}^q - 2F_{n-1}^q - E_{n-1}^q + C_{n-1}^q = 0$ and $G_{n-1} = I_{n-1}$. By analyzing the expressions of the different g_{n-1} given above, it emerges that at the Curie temperature T_c, the probability of having a spin up or down may be equal. Such results have been obtained in Ref. [18] on the Bethe Lattice. Technically, for fixed values of q and sublattice anisotropies, we simply compute $\delta M_A/\delta T$ and

$\delta M_B/\delta T$ as functions of the temperature with $\delta T/J$ set to 10^{-3}. These new curves simultaneously show a maximum at the same temperature that we take as T_c when no anomalous behaviour is observed in the thermal behaviour of F at this moment. We test the validity of such a consideration by computing, using this method, $T_c(\Delta/J, q)$ for $q = 3$ in the model of Ref. [13] and very good agreement was obtained. The FOT is obtained when a sharp jump occurs in the thermal behaviours of the sublattice magnetizations followed by a discontinuity of the first derivative of F.

3. Transition temperatures and phase diagrams

3.1. The $T = 0$ phase diagram

From the expression of the hamiltonian, the energy of a nearest-neighbour spin pair $\langle s, \sigma \rangle$ may be written as:

$$H_L(s, \sigma) = -Js\sigma + \frac{1}{q}\left(\Delta_1 s^2 + \Delta_2 \sigma^2\right). \qquad (14)$$

Due to the ferromagnetic coupling, only six possible pairs with up spins may be considered. Computational analysis of the corresponding energies in the reduced crystal-fields plane $(D_A/q, D_B/q)$ yields the phase diagram displayed in Fig. 2. This diagram shows some key features, in particular, the existence of triple points and coexistence lines where the spin pair energy of some phases coincides. For a given value of q, $D_B = 0$ and increasing D_A, five saturation values exist for M_A whereas for M_B, $\frac{3}{2}$ is the only one saturation value. Thus, we get the thermodynamic phases $\left(\frac{5}{2}, \frac{3}{2}\right)$, $\left(\frac{3}{2}, \frac{3}{2}\right)$, $\left(\frac{1}{2}, \frac{3}{2}\right)$ and at the borders of these phases, two hybrid phases: $\left(2, \frac{3}{2}\right)$, $\left(1, \frac{3}{2}\right)$ at the coexistence points $D_A = \frac{3}{8}q$ and $D_A = \frac{3}{4}q$. These hybrid phases should correspond to the cases where the sublattice A is half-half covered by spins of the two neighbouring phases. It is worthwhile to mention that in the diagram, there are phases where the saturation value of M_B is higher than that of M_A. At large values of the reduced crystal-fields, both magnetizations have the same saturation value 1/2. Along the D_B-axis in the diagram, three saturations values exist due to the same reason mentioned above.

3.2. Sublattice magnetizations and phase diagrams

Here we present the thermal magnetic properties of the system. In Fig. 3, we have depicted the thermal variation of the sublattice magnetizations M_A and M_B as functions of the temperature for two values of the coordination

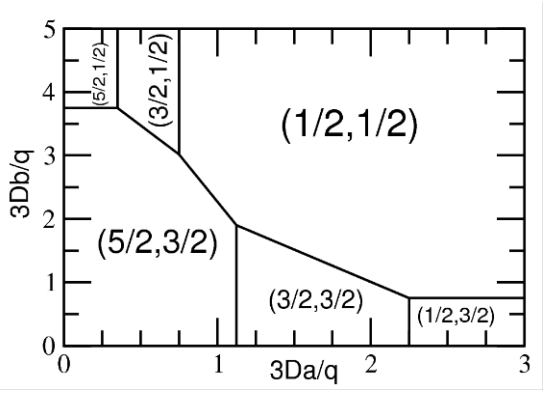

Figure 2. Phase diagram of the model at zero temperature. It shows the different thermodynamic stable phases. Triple points and coexistence lines are present. Along the D_A/q-axis, five saturation values are found for the magnetization of sublattice A whereas along the D_B/q-axis, only three saturation values exist for the magnetization of the sublattice B (see text).

number q and the reduced crystal-field D_A when D_B is set to zero. The results are in perfect agreement with the $T = 0$ phase diagram concerning the saturation values. Indeed, M_B falls from its unique saturation value 3/2 to zero with increasing T whereas M_A shows five saturation values. For both values of q, the curves of M_A and M_B are quite similar to each other and we expect that it should be the case for other values of q. They are all continuous curves of the temperature T. When going from $q = 3$ to $q = 4$, the temperature T_c at which the transition to the disordered phase (with zero net magnetization) occurs is rejected to higher temperatures whereas with increasing D_A, the opposite holds. Thus, T_c is a decreasing function of T. However, for large values of D_A, T_c is almost constant for a given q and this appears clear from the phase diagram illustrated in Fig. 5a. The critical lines of this figure behave as in the phase diagram of Ref. [13]. We check that for $D_A = 0$ and varying D_B, the results are almost similar to the previous ones. One question is how do D_A or D_B alone disorder the system? The answer is given in Fig. 5b. D_A creates much disorder than D_B. In fact, the volume of the ferromagnetic phase for $D_A = 0$ is bigger than the case where $D_B = 0$. This could be explained by the large number of spin states affected by the lattice dynamics when $D_B = 0$.

The model becomes interesting with non-zero values of the reduced crystal-fields D_A and D_B. In particular, when they have values around 1.5 (see below). In Fig. 4a, we have displayed results of M_A and M_B when D_A and D_B have equal strength. At $D_A = 1.0$, M_A and M_B drop repectively from 5/2 and 3/2 which are saturation values. Here the transition to the paramagnetic phase is very sharp but

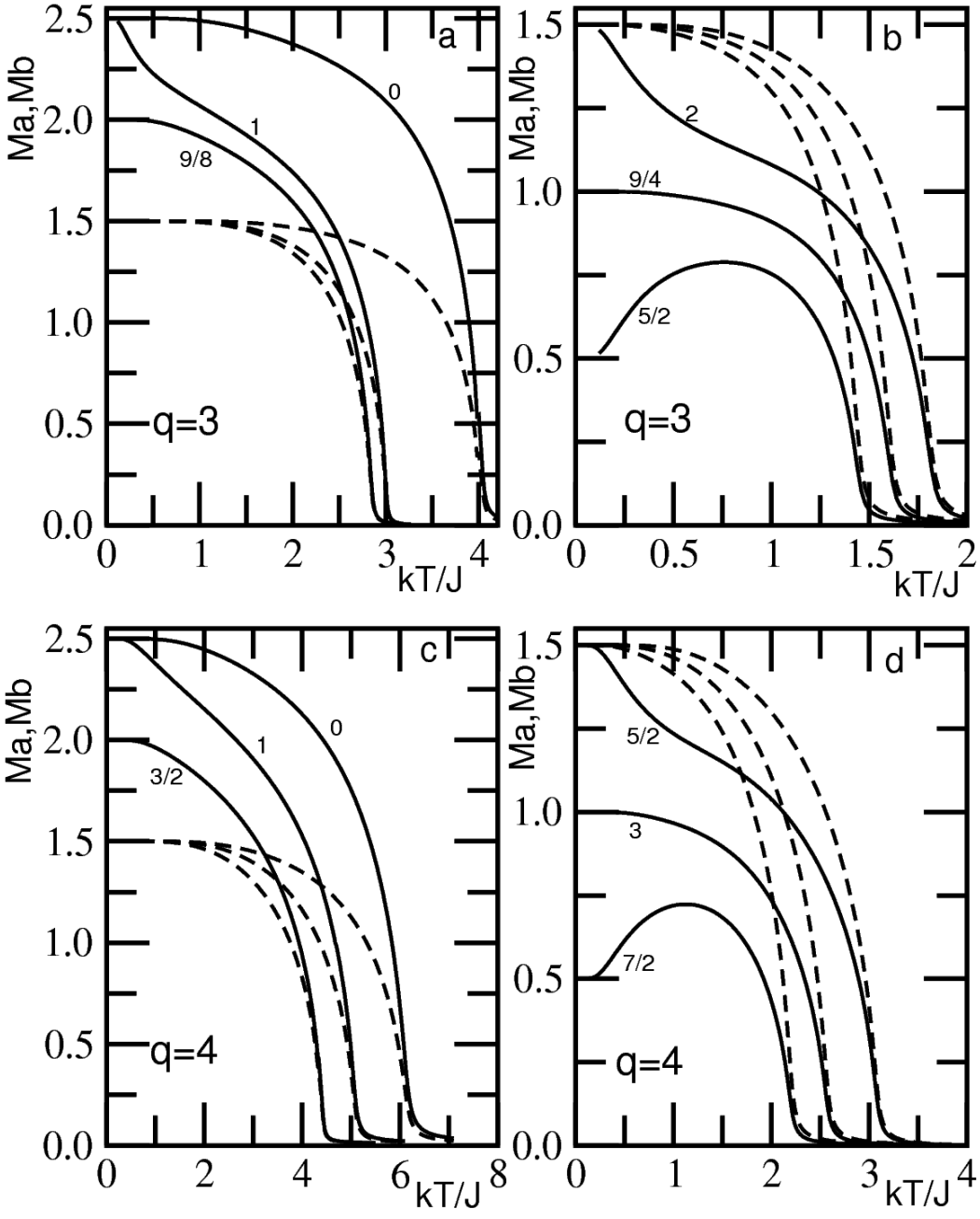

Figure 3. Magnetizations M_A (lines) and M_B (dashed lines) as functions of the reduced temperature kT/J and $q = 3, 4$ in the mixed spin-$\frac{5}{2}$ and spin-$\frac{3}{2}$ model introduced in this work. Curves are displayed for $D_B = 0$ and several values of D_A written on the curves.

not followed by an anomalous behaviour of the free energy. Therefore, we do have a ferro-para SOT. The SOT becomes sharper and sharper when D_B increases. At $D_A = D_B = 1.7$ and increasing T, both magnetizations start at the saturation value 1/2, then jump together to the saturation value 3/2. In other words, the system jumps from the phase (1/2, 1/2) to (3/2, 3/2) and the magnetizations evolve later to zero. The behaviour of the free

energy is also interesting (see Fig. 4b). This energy is almost ∞ at very low temperature, then decreases to $-\infty$ at the jump and later increases to saturate towards zero. Clearly, the free energy is not analytic at the jump's temperature. This is of course a deep sign of a FOT. As we show in Figs. 5c, d, the FOT temperature exists for some appropriate values of $D_A = D_B$. The corresponding transition line (dashed line) approaches the SOT line (full line) but does not connect to it. It tends closer and closer to the SOT line with decreasing q. Unfortunately, at $q = 3$, this line ends at $D_A = D_B = 1.487182$ far from the corresponding SOT temperature. One should expect a link at lower values of q, but the only one existing value is $q = 2$ and this case cannot display reliable physical properties. Accordingly, our calculations do not show the existence of tricritical point where the SOT and the FOT lines meet in the present model. The very low-temperature calculations of the FOT lines meets sometimes some non-convergence problems of the recursion relations. These lines meet the D_A-axis at the values found in Fig. 2. Above the different SOT lines, the system is disordered whereas below, an ordered ferromagnetic phase should prevail. The ordered phase can change from one region to another. At large values of D_A of D_B where the SOT lines become parallel to the D_A-axis, the system remains in the (1/2, 1/2) phase. At small values, we have either (5/2, 3/2) or (3/2, 3/2). Thus, the FOT lines separate three ordered phases as found along the D_A-axis in Fig. 2. Our calculations never show a particular transition from the phase (1/2, 1/2) to the phase (5/2, 3/2). The different results outlined above concerning the $T \neq 0$-phase diagrams bear some resemblance with those reported in Ref. [18] on the Bethe lattice, although the system and the interaction hamiltonian are quite different.

We are now interested in the case where the two crystal-field interactions are dependent in the sense that when D_A takes large values, D_B should be small or vice-versa. One simple way to make such investigations is to set $\Delta_1 = p$ and $\Delta_2 = 1 - p$ where p is a positive real parameter with values between 0 and 1. Results are already displayed for some trivial values of the parameter: $p = 1$ and $p = 0$. For the intermediate values, we make calculations that yield the phase diagram of Fig. 6. The critical line is a decreasing function of p/J; such result is in agreement with the disordering role of D_A stated above.

3.3. The magnetic exponent β_0

The whole magnetization M of the lattice might be $|M_A - M_B|$ or $|M_A + M_B|$. For $D_A = D_B = D$, M_A and M_B have approximately the same behaviour with T when $T \to T_c$. This enables us to extract the magnetic exponent $\beta_0(D)$ from the relation $M \sim t^{\beta_0(D)}$ with $t = |T - T_c|$ when $T \to T_c$ by using M_A or M_B. We study the behaviour of β_0 as a function of the strength D of the sublattice anisotropy. As it could be seen from Fig. 7, the log-log plots of M_A for some values of D, yield straight lines whose slopes determine the values of the exponent β_0. The trend of β_0 with D seems interesting. In fact, at $D = 0$, $\beta_0 = 0.255 \pm 0.009$ and this value of the exponent does not change too much up to $D = 0.5$ (see Fig. 7b). Then $\beta_0(D)$ decreases linearly towards 0 and at $D = 1.5$, we fitted $\beta_0 = 0.0266 \pm 0.0002$. In this region, $\beta_0 \sim (-0.16893 \pm 0.02133).D + 0.27429$. For $D > 1.5$, β_0 starts to increase linearly: $\beta_0 \sim (0.4693 \pm 0.0232).D - 0.6733$, and saturates for D greater than 2.5. At $D = 2.5$, $\beta_0 = 0.4825 \pm 0.0005$ and at $D = 3$, $\beta_0 = 0.4947 \pm 0.0012$. The behaviour of $\beta_0(D)$ could be summarized as follows. For $D < 0.5$, the exponent $\beta_0 = \frac{1}{4}$ and the effect of the lattice anisotropy is marginal on the critical behaviour of the model: the model still behaves as the Ising model spin-5/2 without lattice anisotropy. For $D > 2.5$, the critical

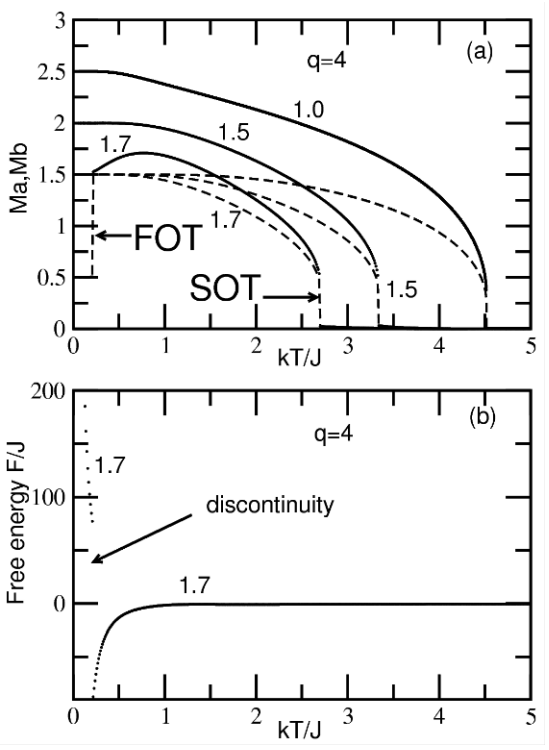

Figure 4. Magnetizations M_A (lines) and M_B (dashed lines) as functions of the reduced temperature kT/J at $q = 4$ in the case where both crystal-fields have the same values ($D_A = D_B$) which are written on the curves (a). In (b), the thermal behaviour of the Helmoltz free energy F/J of the system is illustrated for the crystal-field value $D_A = D_B = 1.7$. Discontinuity appears both in the free energy and in the two magnetizations at the first-order phase transition (FOT).

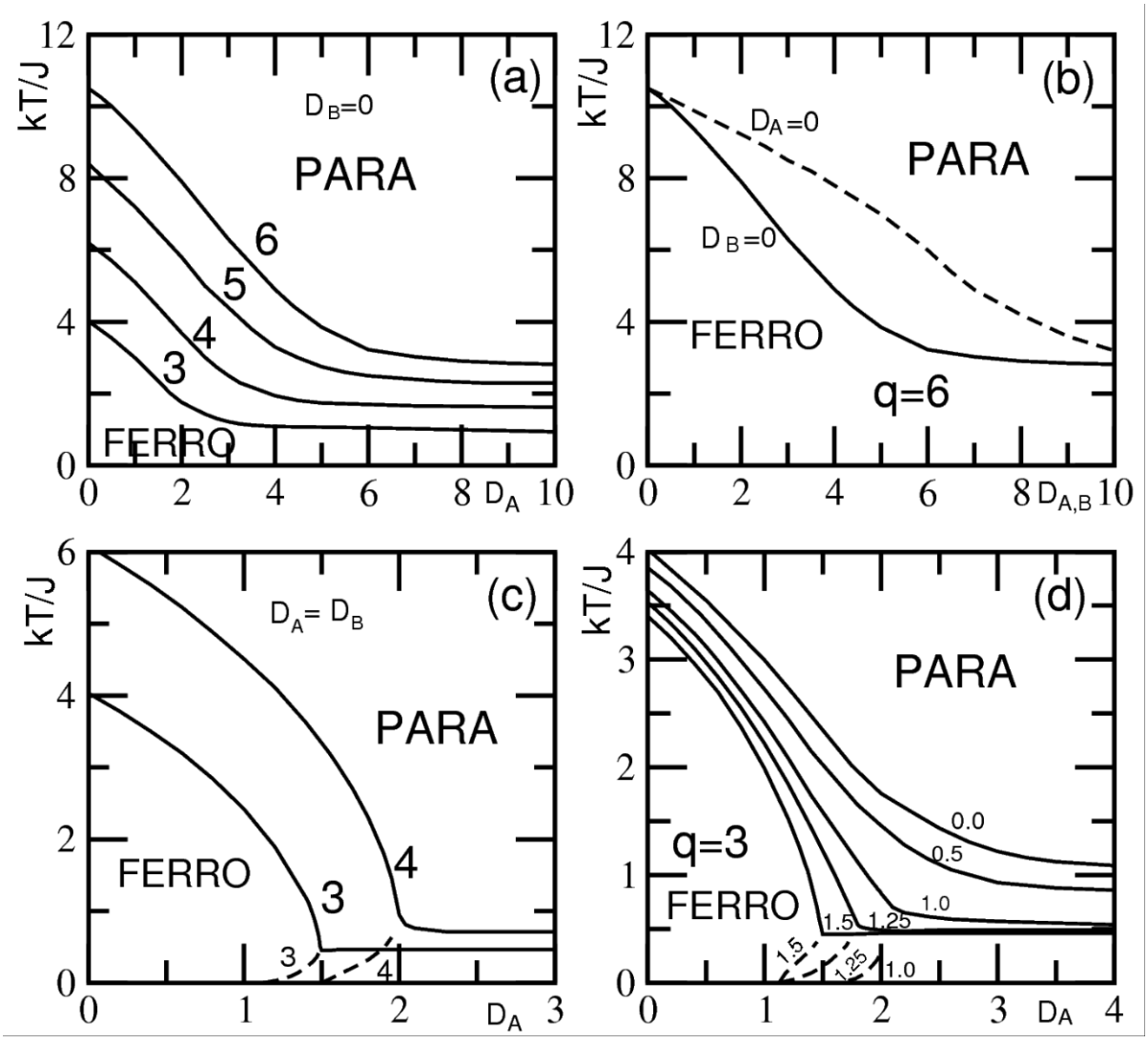

Figure 5. Phase diagram of the mixed spin-$\frac{5}{2}$ and spin-$\frac{3}{2}$ model for $D_B = 0$ (a). The second-order transition (SOT) lines are displayed for several values of the coordination numbers q written on the curves. Above the lines, paramagnetic phase exists whereas below, ordered ferromagnetic phase should prevail. All the curves show the same qualitative similarities. In (b), the phase diagram helps to analyze the disordering effect of each sublattice crystal-field. The case $D_B = 0$ creates much disorder than the case $D_A = 0$. In (c), the phase diagram is given for equal values of both crystal-fields at $q = 3$ and $q = 4$ written on the curves. Full lines are the SOT lines whereas dashed lines correspond to the FOT lines. The FOT lines exist at low temperatures and do not meet the SOT lines. These different critical lines are plotted for several values of D_B written on the curves and for $q = 3$. For other values of q, qualitative similarities are expected. In (d), the diagrams are obtained for constant values of D_B (written on the curves) and $q = 3$.

behaviour is completely different with $\beta_0 = \frac{1}{2}$. There is a crossover between these two different critical behaviours where β_0 first decreases then increases linearly. These results could be interpretated as follows: at very small values of D, the ground state configuration is $\left(\frac{5}{2}, \frac{3}{2}\right)$ or $\left(\frac{3}{2}, \frac{3}{2}\right)$ whereas for large values of D the ground state configuration is $\left(\frac{1}{2}, \frac{1}{2}\right)$. The paramagnetic phase is reached differently from these two phases as the values of the magnetic exponent β_0 are different. Although more calculations are needed to clarify these two universality classes, the present investigation reveals some critical properties of the model and shows that the study of the criticality of Ising systems on hierarchical graphs may be very interesting. One relevant question is whether β_0 still has the same behaviour when $D_A \neq D_B$. Our calculations show that for small values of D_A, β_0 could also be extracted

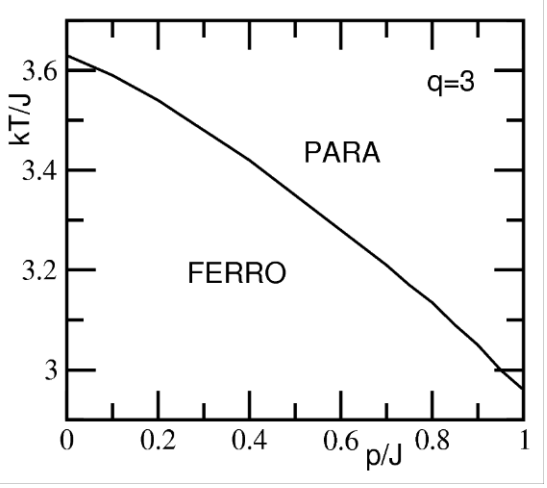

Figure 6. Phase diagram of the model for $q = 3$ when the sublattice crystal-fields are dependent, varying from the value 0 to 1 as defined in the text.

from linear log-log plots of M_A or M_B. Beyond, the plots are not actually linear and real difficulties emerged to estimate reliable values the exponent.

4. Conclusion

We have studied the molecular magnetism of the mixed spin-5/2 and spin-3/2 Blume-Capel Ising ferromagnetic model on the two-fold Cayley tree by means of exact recursion relations. The magnetizations of the two sublattices are calculated and have shown, in most cases, the usual decay with thermal fluctuations. Using the thermal behaviours of these magnetizations and the analyticity or the non-analyticity of the Helmoltz free energy, the nature of the different phase transitions encountered is identified. First-order and second-order phase transitions are found. The range of the first-order phase transition is limited in the physical parameters' space. This transition is completely absent when one of the sublattice anisotropies is zero or very small. Thus, the model compared to the one studied in Ref. [13], presents richer phase diagrams with the existence of first-order transition lines. With increasing coordination number q, it emerged that the critical temperature occur at higher temperatures. However, the phase diagrams have presented qualitative similarities. The critical behaviour of the sublattice magnetization is investigated by extracting the magnetic

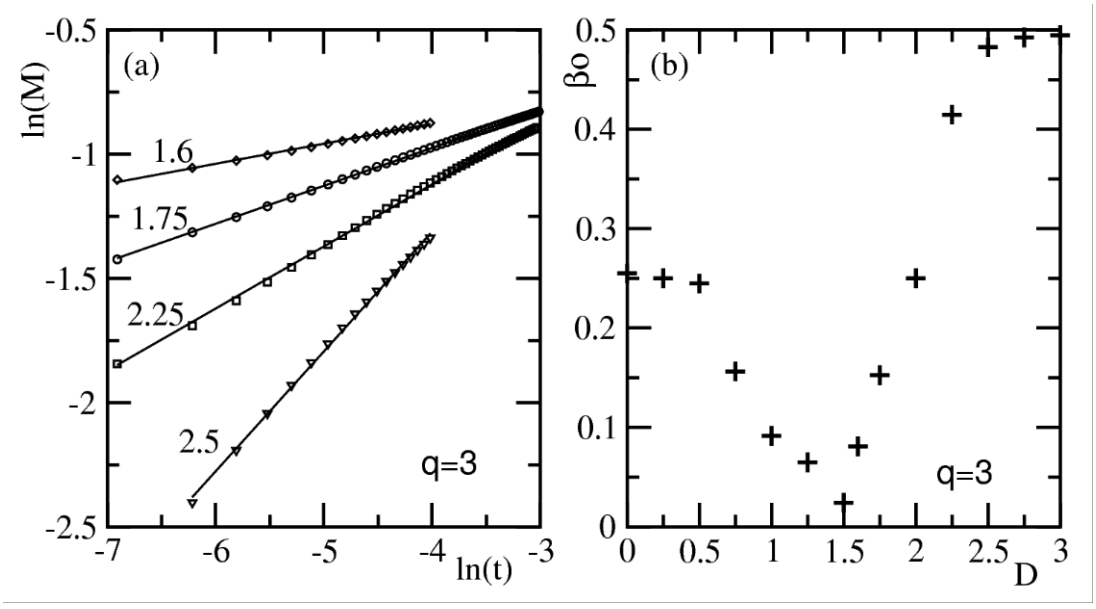

Figure 7. Behaviour of the magnetic exponent β_0 as a function of the parameter $D_A = D_B = D$. In (a), we display log-log plots of M_A as a function of t when $T \to T_c$ at several values of D written on the curves. As shown in the figure, the curves are straight lines and this enables us to fit the corresponding values of the exponent β_0 (see text). In (b), β_0 is given as a function of D and shows two saturation values $\frac{1}{4}$ and $\frac{1}{2}$.

exponent β_0 as a function of the sublattice anisotropy in the case of equal strength $D_A = D_B = D$. Our calculations yielded $\beta_0 = \frac{1}{4}$ at small values of D and $\beta_0 = \frac{1}{2}$ for large values of D. At intermediate values, $\beta_0(D)$ behaves linearly with D. More calculations are certainly needed to completely reveal the richness of the criticality of the model shown in the present investigation.

Acknowledgements

The authors thank Profs. A. C. Levi (University of Genoa, Italy) and M. Marsili (ICTP, Trieste, Italy) for useful comments on the manuscript. F H. is a Senior Associate of the Abdus Salam ICTP, Trieste (Italy).

Appendix A: On the recursion relations

Let us write in the following forms, some of the new variables introduced in subsection IIB:

$$\begin{aligned}
J_n &= \frac{J'_n}{J^0_n}; \quad K_n = \frac{K'_n}{J^0_n}; \quad L_n = \frac{L'_n}{J^0_n}; \quad M_n = \frac{M'_n}{J^0_n}; \quad N_n = \frac{N'_n}{J^0_n} \\
O_n &= \frac{O'_n}{J^0_n}; \quad P_n = \frac{P'_n}{J^0_n}; \quad Q_n = \frac{Q'_n}{J^0_n}; \quad R_n = \frac{R'_n}{J^0_n}; \quad S_n = \frac{S'_n}{J^0_n} \\
T_n &= \frac{T'_n}{J^0_n}; \quad U_n = \frac{U'_n}{J^0_n}; \quad W_n = \frac{W'_n}{J^0_n}; \quad X_n = \frac{X'_n}{J^0_n}; \quad Y_n = \frac{Y'_n}{J^0_n} \\
Z_n &= \frac{Z'_n}{J^0_n}; \quad \gamma_n = \frac{\gamma'_n}{J^0_n}; \quad \beta_n = \frac{\beta'_n}{J^0_n}; \quad \alpha_n = \frac{\alpha'_n}{J^0_n}.
\end{aligned}$$

Thus, the explicit expression of J_n as an example, is obtained from the following expressions of J'_n and J^0_n:

$$\begin{aligned}
J'_n &= e^{\beta\left(\frac{15}{2}J-\frac{9}{2}\Delta_2\right)} + 2e^{-\frac{9}{2}\beta\Delta_2}A^{q-1}_{n-1} + 2e^{\beta\left(5J-\frac{5}{2}\Delta_2\right)}B^{q-1}_{n-1} + 2e^{\beta\left(\frac{5J}{2}-\frac{5}{2}\Delta_2\right)}C^{q-1}_{n-1} + e^{\beta\left(-\frac{15}{2}J-\frac{9}{2}\Delta_2\right)}D^{q-1}_{n-1} \\
&\quad + 2e^{\beta\left(-\frac{5J}{2}-\frac{5}{2}\Delta_2\right)}E^{q-1}_{n-1} + 2e^{\beta\left(-5J-\frac{5}{2}\Delta_2\right)}F^{q-1}_{n-1} + e^{\beta\left(\frac{5}{2}J-\frac{1}{2}\Delta_2\right)}G^{q-1}_{n-1} + 2e^{-\frac{1}{2}\beta\Delta_2}H^{q-1}_{n-1} \\
&\quad + e^{\beta\left(-\frac{5}{2}J-\frac{1}{2}\Delta_2\right)}I^{q-1}_{n-1},
\end{aligned}$$

$$\begin{aligned}
J^0_n &= e^{\beta\left(-\frac{3}{2}J-\frac{9}{2}\Delta_2\right)} + 2e^{-\frac{9}{2}\Delta_2}A^{q-1}_{n-1} + 2e^{\beta\left(-J-\frac{5}{2}\Delta_2\right)}B^{q-1}_{n-1} + 2e^{\beta\left(-\frac{1}{2}J-\frac{5}{2}\Delta_2\right)}C^{q-1}_{n-1} + e^{\beta\left(\frac{3}{2}J-\frac{9}{2}\Delta_2\right)}D^{q-1}_{n-1} \\
&\quad + 2e^{\beta\left(\frac{1}{2}J-\frac{5}{2}\Delta_2\right)}E^{q-1}_{n-1} + 2e^{\beta\left(J-\frac{5}{2}\Delta_2\right)}F^{q-1}_{n-1} + e^{\beta\left(-\frac{1}{2}J-\frac{1}{2}\Delta_2\right)}G^{q-1}_{n-1} + 2e^{-\frac{1}{2}\Delta_2}H^{q-1}_{n-1} + e^{\beta\left(\frac{1}{2}J-\frac{1}{2}\Delta_2\right)}I^{q-1}_{n-1}.
\end{aligned}$$

As above, let us define:

$$\begin{aligned}
A_{n-1} &= \frac{A'_{n-1}}{A^0_{n-1}}; \quad B_{n-1} = \frac{B'_{n-1}}{A^0_{n-1}}; \quad C_{n-1} = \frac{C'_{n-1}}{A^0_{n-1}}; \quad D_{n-1} = \frac{D'_{n-1}}{A^0_{n-1}}; \quad E_{n-1} = \frac{E'_{n-1}}{A^0_{n-1}}; \\
F_{n-1} &= \frac{F'_{n-1}}{A^0_{n-1}}; \quad G_{n-1} = \frac{G'_{n-1}}{A^0_{n-1}}; \quad H_{n-1} = \frac{H'_{n-1}}{A^0_{n-1}}; \quad I_{n-1} = \frac{I'_{n-1}}{A^0_{n-1}}.
\end{aligned}$$

For A_{n-1} as an example, the expressions of A'_{n-1} and A^0_{n-1} are:

$$\begin{aligned}
A'_{n-1} &= e^{-\frac{25\Delta_1 J}{2}} J_{n-2}^{q-1} + \left\{e^{-\frac{15\beta J}{2}} + e^{\frac{15\beta J}{2}}\right\} e^{-\frac{25\beta\Delta_1}{2}} K_{n-2}^{q-1} + \left\{e^{-\frac{3\beta J}{2}} + e^{\frac{3\beta J}{2}}\right\} e^{-\frac{17\beta\Delta_1}{2}} L_{n-2}^{q-1} \\
&+ \left\{e^{-6\beta J} + e^{6\beta J}\right\} e^{-\frac{17\beta\Delta_1}{2}} M_{n-2}^{q-1} + \left\{e^{-3\beta J} + e^{3\beta J}\right\} e^{-\frac{13\beta\Delta_1}{2}} N_{n-2}^{q-1} + \left\{e^{-\frac{9\beta J}{2}} + e^{\frac{9\beta J}{2}}\right\} e^{-\frac{13\beta\Delta_1}{2}} O_{n-2}^{q-1} \\
&+ e^{-\frac{25\beta\Delta_1}{2}} P_{n-2}^{q-1} + \left\{e^{-6\beta J} + e^{6\beta J}\right\} e^{-\frac{17\beta\Delta_1}{2}} Q_{n-2}^{q-1} + \left\{e^{-\frac{3\beta J}{2}} + e^{\frac{3\beta J}{2}}\right\} e^{-\frac{17\beta\Delta_1}{2}} R_{n-2}^{q-1} \\
&+ \left\{e^{-\frac{9\beta J}{2}} + e^{\frac{9\beta J}{2}}\right\} e^{-\frac{13\beta\Delta_1}{2}} S_{n-2}^{q-1} + \left\{e^{-3\beta J} + e^{3\beta J}\right\} e^{-\frac{13\beta\Delta}{2}} T_{n-2}^{q-1} + e^{-\frac{9\beta\Delta_1}{2}} U_{n-2}^{q-1} \\
&+ \left\{e^{-\frac{9\beta J}{2}} + e^{\frac{9\beta J}{2}}\right\} e^{-\frac{9\beta\Delta_1}{2}} V_{n-2}^{q-1} + \left\{e^{-\frac{3\beta J}{2}} + e^{\frac{3\beta J}{2}}\right\} e^{-\frac{5\beta\Delta_1}{2}} W_{n-2}^{q-1} + \left\{e^{-3\beta J} + e^{3\beta J}\right\} e^{-\frac{5\beta\Delta_1}{2}} X_{n-2}^{q-1} \\
&+ e^{-\frac{9\beta\Delta}{2}} Y_{n-2}^{q-1} + \left\{e^{-3\beta J} + e^{3\beta J}\right\} e^{-\frac{5\beta\Delta_1}{2}} Z_{n-2}^{q-1} + \left\{e^{-\frac{3\beta J}{2}} + e^{\frac{3\beta J}{2}}\right\} e^{-\frac{5\beta\Delta_1}{2}} \gamma_{n-2}^{q-1} + e^{-\frac{\beta\Delta_1}{2}} \beta_{n-2}^{q-1} \\
&+ \left\{e^{-\frac{3\beta J}{2}} + e^{\frac{3\beta J}{2}}\right\} e^{-\frac{\beta\Delta_1}{2}} \alpha_{n-2}^{q-1} + e^{-\frac{\beta\Delta_1}{2}},
\end{aligned}$$

$$\begin{aligned}
A^0_{n-1} &= e^{-\frac{15\beta J}{2}} e^{-\frac{25\beta\Delta_1}{2}} J_{n-2}^{q-1} + 2e^{-\frac{25\beta\Delta_1}{2}} K_{n-2}^{q-1} + 2e^{6\beta J} e^{-\frac{17\beta\Delta_1}{2}} L_{n-2}^{q-1} + 2e^{\frac{3\beta J}{2}} e^{-\frac{17\beta\Delta_1}{2}} M_{n-2}^{q-1} \\
&+ 2e^{\frac{9\beta J}{2}} e^{-\frac{13\beta\Delta_1}{2}} N_{n-2}^{q-1} + 2e^{3\beta J} e^{-\frac{13\beta\Delta_1}{2}} O_{n-2}^{q-1} + e^{-\frac{15\beta J}{2}} e^{-\frac{25\beta\Delta_1}{2}} P_{n-2}^{q-1} + 2e^{-\frac{3\beta J}{2}} e^{-\frac{17\beta\Delta_1}{2}} Q_{n-2}^{q-1} \\
&+ 2e^{-6\beta J} e^{-\frac{17\beta\Delta_1}{2}} R_{n-2}^{q-1} + 2e^{-3\beta J} e^{-\frac{13\beta\Delta_1}{2}} S_{n-2}^{q-1} + 2e^{-\frac{9\beta J}{2}} e^{-\frac{13\beta\Delta_1}{2}} T_{n-2}^{q-1} + e^{\frac{9\beta J}{2}} e^{-\frac{9\beta\Delta_1}{2}} U_{n-2}^{q-1} \\
&+ 2e^{-\frac{9\beta\Delta_1}{2}} V_{n-2}^{q-1} + 2e^{3\beta J} e^{-\frac{5\beta\Delta_1}{2}} W_{n-2}^{q-1} + 2e^{\frac{3\beta J}{2}} e^{-\frac{5\beta\Delta_1}{2}} X_{n-2}^{q-1} + e^{-\frac{9\beta J}{2}} e^{-\frac{9\beta\Delta_1}{2}} Y_{n-2}^{q-1} + 2e^{-\frac{3\beta J}{2}} e^{-\frac{5\beta\Delta_1}{2}} Z_{n-2}^{q-1} \\
&+ 2e^{-3\beta J} e^{-\frac{5\beta\Delta_1}{2}} \gamma_{n-2}^{q-1} + e^{\frac{3\beta J}{2}} e^{-\frac{\beta\Delta_1}{2}} \beta_{n-2}^{q-1} + 2e^{-\frac{\beta\Delta_1}{2}} \alpha_{n-2}^{q-1} + e^{-\frac{3\beta J}{2}} e^{-\frac{\beta\Delta_1}{2}}.
\end{aligned}$$

Appendix B: On the expression of the free energy F

The expression of F is obtained from the following terms:

$$\begin{aligned}
f_1 &= e^{\frac{\beta}{2}(15J-25\Delta_1)} J_n^{q-1} + 2e^{\left(-\frac{25}{2}\beta\Delta_1\right)} K_n^{q-1} + 2e^{\beta\left(6J-\frac{17}{2}\Delta_1\right)} L_n^{q-1} + 2e^{\frac{\beta}{2}(3J-17\Delta_1)} M_n^{q-1}, \\
f_2 &= 2e^{\frac{\beta}{2}(9J-13\Delta_1)} N_n^{q-1} + 2e^{\beta\left(3J-\frac{13}{2}\Delta_1\right)} O_n^{q-1} + e^{-\frac{\beta}{2}(15J+25\Delta_1)} P_n^{q-1} + 2e^{-\frac{\beta}{2}(3J+17\Delta_1)} Q_n^{q-1}, \\
f_3 &= 2e^{-\beta\left(6J+\frac{17}{2}\Delta_1\right)} R_n^{q-1} + 2e^{-\beta\left(3J+\frac{13}{2}\Delta_1\right)} S_n^{q-1} + 2e^{-\frac{\beta}{2}(9J+13\Delta_1)} T_n^{q-1} + e^{\frac{\beta}{2}(9J-9\Delta_1)} U_n^{q-1}, \\
f_4 &= 2e^{-\frac{9}{2}\beta\Delta_1} V_n^{q-1} + 2e^{\beta\left(3J-\frac{5}{2}\Delta_1\right)} W_n^{q-1} + 2e^{\frac{\beta}{2}(3J-5\Delta_1)} X_n^{q-1} + e^{\frac{-\beta}{2}(9J+9\Delta_1)} Y_n^{q-1}, \\
f_5 &= 2e^{-\frac{\beta}{2}(3J+5\Delta_1)} Z_n^{q-1} + 2e^{-\beta\left(3J+\frac{5}{2}\Delta_1\right)} \gamma_n^{q-1} + e^{\frac{\beta}{2}(3J-\Delta_1)} \beta_n^{q-1} + 2e^{-\frac{1}{2}\beta\Delta_1} \alpha_n^{q-1} + e^{\frac{-\beta}{2}(3J+\Delta_1)}, \\
f_6 &= e^{-\frac{25\beta}{2}\Delta_1} J_n^q + 2e^{-\frac{25}{2}\beta\Delta_1} K_n^q + 2e^{-\frac{17}{2}\beta\Delta_1} L_n^q + 2e^{-\frac{17\beta}{2}\Delta_1} M_n^q, \\
f_7 &= 2e^{-\frac{13\beta}{2}\Delta_1} N_n^q + 2e^{-\frac{13}{2}\beta\Delta_1} O_n^q + e^{-\frac{25\beta}{2}\Delta_1} P_n^q + 2e^{-\frac{17\beta}{2}\Delta_1} Q_n^q, \\
f_8 &= 2e^{-\frac{17}{2}\beta\Delta_1} R_n^q + 2e^{-\frac{13}{2}\beta\Delta_1} S_n^q + 2e^{-\frac{13}{2}\beta\Delta_1} T_n^q + e^{-\frac{9}{2}\beta\Delta_1} U_n^q, \\
f_9 &= 2e^{-\frac{9}{2}\beta\Delta_1} V_n^q + 2e^{-\frac{5}{2}\beta\Delta_1} W_n^q + 2e^{-\frac{5}{2}\beta\Delta_1} X_n^q + e^{-\frac{9}{2}\beta\Delta_1} Y_n^q, \\
f_{10} &= 2e^{-\frac{5}{2}\beta\Delta_1} Z_n^q + 2e^{-\frac{5}{2}\beta\Delta_1} \gamma_n^q + e^{-\frac{1}{2}\beta\Delta_1} \beta_n^q + 2e^{-\frac{1}{2}\beta\Delta_1} \alpha_n^q + e^{-\frac{1}{2}\beta\Delta_1}, \\
f_{11} &= e^{-\frac{\beta}{2}(3J+9\Delta_2)} + 2e^{\left(-\frac{9}{2}\beta\Delta_2\right)} A_{n-1}^{q-1} + 2e^{-\beta\left(J+\frac{5}{2}\Delta_2\right)} B_{n-1}^{q-1} + 2e^{-\frac{\beta}{2}(J+5\Delta_2)} C_{n-1}^{q-1}, \\
f_{12} &= e^{\frac{\beta}{2}(3J-9\Delta_2)} D_{n-1}^{q-1} + 2e^{\frac{\beta}{2}(J-5\Delta_2)} E_{n-1}^{q-1} + 2e^{\beta\left(J-\frac{5}{2}\Delta_2\right)} F_{n-1}^{q-1} + e^{-\frac{\beta}{2}(J+\Delta_2)} G_{n-1}^{q-1}, \\
f_{13} &= 2e^{\left(-\frac{1}{2}\beta\Delta_2\right)} H_{n-1}^{q-1} + e^{\frac{\beta}{2}(J-\Delta_2)} I_{n-1}^{q-1}, \\
F_1 &= f_1 + f_2 + f_3 + f_4 + f_5, \qquad F_2 = f_6 + f_7 + f_8 + f_9 + f_{10}, \qquad F_3 = f_{11} + f_{12} + f_{13}.
\end{aligned}$$

The explicit expression of the free energy of the system reads:

$$\frac{F}{J} = \frac{1}{\beta J}\left\{\frac{q-1}{2-q}\ln F_1 + \ln F_2 + \frac{1}{2-q}\ln F_3\right\}.$$

References

[1] O. Khan, Molecular Magnetism (VCH, New-York, 1993)
[2] M. Monsuripur, J. Appl. Phys. 61, 1580 (1987)
[3] C. Ekiz, M. Keskin, Physica A 317, 517 (2003)
[4] C. Ekiz, Physica A 347, 353 (2005)
[5] A. Dakhama, N. Benayad, J. Magn. Magn. Mater. 213, 213 (2000)
[6] A. Dakhama, Physica A 252, 225 (2003)
[7] P. F. Li, Y. G. Chen, H. Chen, Eur. Phys. J. B 51, 473 (2006)
[8] T. Kaneyoshi, J. Phys. Soc. Jpn. 56, 2675 (1987)
[9] T. Kaneyoshi, Physica A 303, 507 (2002)
[10] G. M. Zhang, C. Z. Yang, Phys. Rev. B48, 9452 (1993)
[11] T. W- Tucher, J. Magn. Magn. Mater. 195, 733 (1999)
[12] B. Boechat, R. A. Filgueiras, C. Cordeiro, N. S. Branco, Physica A 304, 429 (2002)
[13] X. Zhang, X.-M. Kong, Physica A 369, 589 (2006)
[14] C. F. Delale, Int. J. Mod. Phys. B 3, 1523 (1989)
[15] E. Albayrak, M. Keskin, Eur. Phys. J. B 24, 505 (2001)
[16] C. Ekiz, J. Magn. Magn. Mater. 293, 759 (2005)
[17] Q. Zhang, G. Wei, W. Gu, Phys. Status Solidi B 242, 924 (2005)
[18] E. Albayrak, A. Yigit, Phys. Lett. A, 353, 121 (2006)